Environmental Science and Pollution Research
https://doi.org/10.1007/s11356-024-34001-6

RESEARCH ARTICLE

Preparation of porous hydroxyapatite–metakaolin geopolymer granules for adsorption applications using polyethylene glycol as porogen agent and sodium dodecyl sulfate as anionic surfactant

Aghilas Brahmi[1,2] · Salima Ziani[1,3] · Salima AitAli[1,3] · Hafit Khireddine[3] · Tero Luukkonen[2,4]

Received: 29 February 2024 / Accepted: 11 June 2024

Abstract

This study investigated the elaboration of novel porous absorbent granules by mixing powdered hydroxyapatite, metakaolin, sodium metasilicate, polyethylene glycol, and sodium dodecyl sulfate (SDS), an anionic surfactant. The effect of sodium dodecyl sulfate (SDS) was then studied by introducing it as a powder to the powdered mixture or dissolved into the granulation fluid. Characterization of the granules indicated that the incorporation of SDS dissolved in the granulation fluid into the G-PEG granules improved their specific surface area (97.9 m^2/g) and porosity, resulting in a synergistic increase in the adsorption of crystal violet and methylene blue dyes compared to G-PEG granules and hydroxyapatite or metakaolin geopolymer alone. Moreover, the granules exhibited satisfactory compressive strength of 0.81 MPa, making them suitable for large-scale adsorption columns. Finally, the regeneration process of the granules was modeled and optimized by using surface response methodology based on Box–Behnken design. The granules could be regenerated for eight cycles under optimum conditions of acetic acid concentration of 0.72 mol/L, a temperature of 323 K, and a contact time of 173.22 min, without a significant loss in the adsorption capacity or degradation of the granules. These results suggest that the porous granules prepared in this study have potential to be used in industrial wastewater treatment.

Keywords Adsorbent granulation · Hydroxyapatite · Geopolymers · Box–Behnken design · Wastewater treatment

Abbreviations

$\alpha_{1/2}$	Separation factor
a_R	Redlich–Peterson isotherm constants (L/mg)
ΔZ_j	Step size
β	Redlich–Peterson isotherm constants
b_0	Value of the fitted response at the center point of the design
b_j	Linear terms
b_{jj}	Quadratic terms
b_{uj}	Interaction terms
BBD	Box–Behnken design
BET	Brunauer-Emmett-Teller
BJH	Barrett-Joyner-Halenda
CCD	Central composite design
C_e	Equilibrium concentration in aqueous (mg/L)
C_s	Equilibrium concentration in solid phase (mg/L)
CV	Crystal violet
d	Diameter of granules (mm)
D_f	Film diffusion coefficient in liquid phase (m2/s)
D_p	Effective diffusion coefficient (m2/s)
DF	Degrees of freedom
DTG	Differential thermal analysis
DSC	Differential scanning calorimetry
ε	Residue
F	Peak force (N)

Responsible Editor: Guilherme Luiz Dotto

Highlights

- A novel, straightforward, and scalable method was developed for the preparation of porous hydroxyapatite–metakaolin geopolymer using polyethylene glycol as a porogen agent.
- The incorporation of sodium dodecyl sulfate (SDS) dissolved in the granulation fluid probably enhanced geopolymer formation by reducing water surface tension.
- The granules prepared with SDS demonstrated significantly enhanced proprieties and synergistic adsorption capacity compared with those prepared solely with HAP or MK-GP and those prepared without SDS.
- Modelization and optimization of the regeneration process parameters of HAP-MK-GP granules using response surface methodology based on Box–Behnken design.
- The obtained granules exhibit enduring, high-stress, and Young's modulus characteristics, making them suitable for use in large-scale adsorption columns.

Extended author information available on the last page of the article

Published online: 20 June 2024

FTIR	Fourier transform infrared spectroscopy
δ	Film thickness (m)
HAP	Hydroxyapatite
HPDM	Homogeneous particle diffusion model
k	Diffusion rate constant (L/s)
k_1	Pseudo-first-order rate constant (min−1)
k_2	Pseudo-second-order rate constant (g/(mg × min))
K_d	Distribution coefficients (L/g)
K_F	Freundlich constants (mg(1–1/n) × L(1/n)/g)
K_L	Langmuir adsorption constant (L/mg)
k_p	Diffusion rate constant (L/s)
K_R	Redlich–Peterson isotherm constants (L/g)
λ_{max}	Maximum emission wavelength (nm)
m	Mass of the adsorbent granules (g)
MB	Methylene blue
MK	Metakaolin
MK-GP	Metakaolin geopolymer
MS	Mean of squares
N	Number of experiments
OFAT	One-factor-at-a-time
PEG	Polyethylene glycol
q_e	Adsorption capacity at equilibrium (mg/g)
q_i^{exp}	Measured adsorption amounts (mg/g)
q_i^{pred}	Predicted values of the adsorption amounts (mg/g)
q_{max}	Langmuir monolayer adsorption capacity (mg/g)
q_t	Adsorption capacity versus time (mg/g)
r_0	Radius of the granules (m)
RMSEC	Root mean square error
RSM	Response surface methodology
SSA	Specific surface area
SEM	Scanning electron microscope
SDS	Sodium dodecyl sulfate
σ	Compressive strength (MPa)
SS	Sum of squares
TGA	Thermogravimetric analysis
UV-Vis	Spectroscopy of the ultraviolet–visible range
V	Volume of the solution (L)
x_j	Dimensionless variables or coded forms that correspond to Z_j
$X_{(t)}$	The fractional adsorption at given time
XRF	X-ray fluorescence spectroscopy
y	Measured dye removal efficiency response
$\hat{y}$	Predicted dye removal efficiency response
Z_j	Dimensionless variables or reel forms
Z_j^0	Value of Z_j at the center point of the investigation domain
Z_{jmax}	Maximum level of factor j in natural units
Z_{jmin}	Minimum level of factor j in natural units
$\frac{1}{n}$	Partitioning coefficient

Introduction

Hydroxyapatite (HAP), a major component of teeth and bones, is the most extensively investigated calcium phosphate ceramic both in biomedical and environmental fields (Meski et al. 2011). HAP exhibits remarkably versatile properties, enabling its use in various applications depending on its microstructure, making it useful in dental implants, scaffolds for tissue engineering, and as an adsorbent in water treatment. HAP can be synthesized using natural resources such as eggshells, shells, fish bones and scales, animal bones, and algae (Teymouri 2018; Ziani et al. 2014). In wastewater treatment, HAP can be used to separate several pollutants with very promising equilibrium adsorption capacities (q_e) such as lead (q_e = 698 mg/g) (Meski et al. 2011), zinc (q_e = 450 mg/g) (Meski et al. 2010), copper (q_e = 91 mg/g) (Wang et al.2017), dyes (methylene blue (q_e = 328 mg/g)) (Peng et al. 2019), Congo red (q_e = 48 mg/g) (Panneerselvam et al. 2019), and acid yellow (q_e = 213 mg/g) (Manatunga et al. 2018). Furthermore, HAP is effective in adsorbing emerging pollutants, such as ofloxacin (q_e = 27 mg/g) and triclosan (q_e = 130 mg/g) (Huang et al. 2016). However, most existing studies have been conducted using powdered HAP, and there is little research on HAP-based granules as adsorbents (Chen 2023).

Geopolymers (GPs) are ceramic-like amorphous aluminosilicates, formed by mixing an aluminosilicate precursor (e.g., metakaolin) with an alkali-activator solution (e.g., sodium silicate). They have been extensively studied in water and wastewater treatment as adsorbents, membrane materials, filtration media, and catalyst support and for solidification/stabilization of solid residues (Al Natsheh et al. 2022; Luukkonen et al. 2020, 2019). Porous GP composites can be produced through direct foaming (i.e., introduction of a blowing agent to produce gas bubbles), addition of lightweight fillers, additive manufacturing, reactive emulsion templating, particle compaction, or mixed approaches (Zhang et al. 2021).

Recent research has explored the possibility of combining HAP powder with a metakaolin GP (MK-GP) via granulation to form adsorbent granules (Brahmi et al. 2024), improving their feasibility for practical water treatment applications. In this study, a novel method for introducing porosity to HAP-MK-GP granules is proposed by using polyethylene glycol (PEG) as a templating agent and sodium dodecyl sulfate (SDS) as an anionic surfactant. This approach aims to enhance the adsorption and surface properties of HAP-MK-GP granules using the anionic structure of SDS, which has hydrophobic and hydrophilic functional groups, allowing it to interact with organic compounds and cationic pollutants, facilitating their removal from aqueous

solutions. In addition, this study investigates the most effective approach to employ SDS, either as powder or as an aqueous granulation fluid to reduce water surface tension during the granulation process, which can enhance the even distribution of water within the granulation mixture components, ultimately improving the granule formation process.

The developed granules are demonstrated as potential adsorbents for dye removal using cationic dyes, methylene blue (MB), and crystal violet (CV), as model adsorbates (either alone or from a binary solution), and their low-cost regeneration is demonstrated and optimized using statistical design of experiments based on response surface methodology (RSM) with Box–Behnken design (BBD).

Materials and methods

Chemicals

The raw materials used to prepare HAP were $Ca(NO_3)_2{\bullet}4H_2O$ (99% assay) and $(NH_4)_2HPO_4$ (99.2% assay) obtained from Biochem Chemopharma (Canada) and Analar Normapur (Belgium), respectively. CV and MB dyes were obtained from Sigma-Aldrich (China). HCl (0.1 N) and NaOH (0.1 N) solutions used to adjust pH were obtained from VWR (Belgium). The raw materials used to prepare porous MK-GP granules were metakaolin (MetaMax, BASF, USA), solid anhydrous sodium metasilicate (Na_2O (50.8 wt%), SiO_2 (46.7 wt%), and H_2O (2.5 wt%); VWR Alfa Aesar, Germany), SDS obtained from SIGM (China), and PEG with an average molar mass of 4000 g/mol obtained from Merck (Germany). Acetic acid (1.0 N) obtained from Sigma-Aldrich (Germany) was used for the regeneration studies.

Preparation of HAP powder

The HAP powder was synthesized using the co-precipitation method described previously in the literature (Brahmi et al. 2024).

Preparation of porous HAP-MK-PEG/SDS granules

Three batches of granules were prepared, which are referred to as G-PEG (i.e., with PEG and without SDS), G-PEG-SDS (S) (i.e., with PEG and SDS added as a solid powder), and G-PEG-SDS (L) (i.e., with PEG and SDS added as an aqueous solution). The performance of reference granules without PEG and SDS has been represented in a previous study by the authors (Brahmi et al. 2024). First, HAP, PEG, sodium metasilicate, metakaolin, and SDS (SDS only in the G-PEG-SDS (S) granules) were mixed as dry powders (Table 1), ground using a disc mill (Retsch RS 200) at a speed of 1500 rpm for 5 min, and then placed in a high-shear granulator (Eirich EL1). Afterward, deionized water (35 mL for a dry solid mass of 80 g) was used as a granulation fluid by adding it dropwise to the granulator using a granulator pan mixing speed of 1200 rpm, granulator mixer plate speed of 170 rpm, and granulator tilting angle of 30°. Granulation was stopped when the granules were formed by visual observation. The G-PEG-SDS (L) granules were prepared by dissolving SDS (Table 1) in the volume of the deionized water ($V = 35$ mL), which was used as a granulation fluid.

Finally, the granules were cured at 333 K for 24 h. They were then cleaned by mixing with distilled water ($V = 200$ mL) at 358 K and a mixing speed of 150 rpm for 5 h to remove PEG contained in the granules (the operation was repeated three times). Subsequently, they were dried in an oven at 333 K for 24 h.

Characterization of granules

The functional groups of the as-prepared granules were identified using Fourier transform infrared spectroscopy (FTIR) in the range of 400–4000 cm^{-1}, with a spectral resolution of 200. Analyses were performed using a Bruker Vertex v80 instrument fitted with a Harrick Praying Mantis DRIFT cell. In addition, the elemental composition of granules was obtained using an X-ray fluorescence spectrometer (XRF) (PanAnalytical Minipal 4).

Thermogravimetric analysis (TGA) and differential thermal gravimetric (DTG) analysis for the HAP and MK powders and elaborated granules were performed using an SDT 650 simultaneous thermal analyzer (a heating rate of 10 °C/min under nitrogen atmosphere).

The specific surface area and pore size were determined using a Micrometrics ASAP2020 instrument and calculated using the Brunauer–Emmett–Teller (BET) isotherm and the Barrett–Joyner–Halenda (BJH) method.

The microstructural morphology and composition of the samples were determined using a field emission scanning electron microscope equipped with an energy dispersive

Table 1 Composition of the elaborated granules

Samples	HAP (g)	MK (g)	Sodium metasilicate (g)	PEG (g)	SDS (g)	H_2O (mL)
G-PEG	61	18	18	3	0	35
G-PEG-SDS (S)	60	18	18	3	1	35
G-PEG-SDS (L)	60	18	18	3	1	35

X-ray spectroscope (FE-SEM–EDS, Zeiss Ultra Plus). In addition, the cross-sections of the granules were imaged using an optical microscope (Leica MZ6 equipped with a Leica DFC420 camera).

The mechanical strength of the granules was determined using a Zwick Roell Z010 (10 kN load cell) instrument with a loading rate of 1 mm/min. The granules selected for the compression test were spherical with a diameter of 4 mm, and measurements were performed for five granules from each batch. The compressive strength (σ, MPa) was calculated using Eq. (1), where F (N) represents the peak force and d (mm) represents the granule diameter.

$$\sigma = 4 \times \frac{F}{\pi \times d^2} \tag{1}$$

Batch adsorption studies

First, a comparative study was conducted for the adsorption efficiency of the granules and HAP and MK-GP powders. Adsorption studies were conducted using MB and CV dyes individually in aqueous solutions under the following conditions: $[\text{dye}]_0 = 25\,\text{mg/L}, \text{pH}=7, \text{granule mass per water volume} = 2\,\text{g/L}, d_{\text{granules}} = 4\,\text{mm}$, agitation speed = 250 rpm, time = 90 min, and $T = 298$ K. After the comparative study, the G-PEG-SDS (L) granules were used subsequently, because they have higher adsorption capacity than the other granules.

The adsorption parameters (i.e., contact time (0–180 min), mass of granules (1–4 g/L), and solution pH (3–10)) were optimized. Then, the selectivity of the granules was evaluated using MB and CV dyes at concentrations ranging from 25 to 180 mg/L in aqueous solutions. In addition, a binary mixture of MB and CV at different concentrations (ranging from 15 to 100 mg/L, with both dyes having the same concentration) was examined. The conditions in the experiments assessing selectivity were as follows: pH of 8, granule diameter of 4 mm, granule mass per water volume of 3 g/L, agitation speed of 250 rpm, contact time up to 180 min, and temperature of 298 K.

After each experiment, the water samples were centrifuged (Beckman Coulter J326XPI-IM-1) at 8000 rpm for 5 min, and the supernatant was collected and analyzed using a UV-6300PC spectrophotometer (VWR, China) at the following wavelengths: $\lambda_{MB} = 664$ nm and $\lambda_{\text{CV}} = 586$ nm. The calibration curves for MB and CV are shown in Figs. S1 and S2 (supporting information). The dye removal efficiency y (%) and the adsorption capacity, q_t (mg/g), of the dyes were calculated using Eqs. (2) and (3), respectively.

$$y(\%) = \frac{[\text{dye}]_0 - [\text{dye}]_t}{[\text{dye}]_0} \times 100, \tag{2}$$

$$q_t = \left([\text{dye}]_0 - [\text{dye}]_t\right) \times \frac{V}{m}, \tag{3}$$

where $[\text{dye}]_0$ and $[\text{dye}]_t$ (mg/L) denote the initial concentrations of the dyes (i.e., MB or CV) and their concentrations at time t, respectively; V (L) represents the volume of the solution; and m (g) represents the mass of the adsorbent granules.

The selectivity of G-PEG/SDS (L) granules toward the two dyes in a binary solution was evaluated using the separation factor ($\alpha_{1/2}$, Eq. (4)), which is defined as the ratio of the equilibrium adsorption constants for the two components (Shen et al. 2018).

$$\alpha_{\frac{1}{2}} = \frac{K_{d,1}}{K_{d,2}} \text{and } K_d = \frac{q_e}{C_e} \tag{4}$$

In Eq. (4), $K_{d,1}$ and $K_{d,2}$(L/g) denote the distribution coefficients of the dyes between the adsorbent surface and solution at the equilibrium, respectively; q_e (mg/g) denotes the adsorption capacity; and C_e (mg/L) denotes the concentration of the MB or CV dyes at equilibrium.

Rate-controlling step of the adsorption of dyes

Homogeneous particle diffusion model (HPDM)

The HPDM shown in Eq. (5), originally introduced by Boyd et al. (Boyd et al. 1947), describes the rate-limiting step, which can be controlled using either an intra-particle or film diffusion mechanism (Benamor et al. 2008).

$$X_{(t)} = \frac{q_t}{q_e} = 1 - \frac{6}{\pi^2} \sum_{z=1}^{\infty} \frac{1}{Z^2} \exp\left[\frac{-Z^2 \pi^2 D_p t}{r_0^2}\right]. \tag{5}$$

To describe the adsorption onto spherical particles and when $0 < X_{(t)} < 1$, Eqs. (6) and (7) are used as simplified equations derived from Eq. (5) (Liu et el. 2008).

$$X_{(t)} = \left[1 - \exp\left[\frac{-\pi^2 D_p^2 t}{r_0^2}\right]\right]^{0.5}, \tag{6}$$

$$-ln\left(1 - X_{(t)}{}^2\right) = 2k_p t = \frac{2\pi^2 D_p}{r_0^2} t, \tag{7}$$

$$\text{with } D_p = \frac{k_p r_0^2}{\pi^2},$$

where $X_{(t)}$ denotes the fractional adsorption at time t, D_p (m^2/s) denotes the effective diffusion coefficient, r_0 denotes

the radius of the granules (0.4×10^{-3} m), Z represents an integer, and k_p denotes the diffusion rate constant (L/s).

When the rate of adsorption is controlled by the liquid film diffusion, Eq. (8) can be used (Liu et el. 2008).

$$-\ln\left(1 - X_{(t)}\right) = k_{li}t = \left[\frac{3D_f C_e}{r_0 \delta C_s}t\right] \tag{8}$$

$$\text{with } D_f = \frac{k_d r_0 \delta C_s}{3C},$$

where D_f (m^2/s) denote the film diffusion coefficient in the liquid phase, k represents the diffusion rate constant (L/s), C_s (mg/L) denotes the equilibrium concentration of MB and CV in the solid phase (granules), and δ denotes the film thickness, which was estimated to 10^{-5} (m) (Yu & Luo 2014).

The graphs of $-\ln\left(1 - X_{(t)}{}^2\right)$ and $-\ln\left(1 - X_{(t)}\right)$ were used to determine the values of K_p and K_f, respectively, for different concentrations of MB and CV dyes in the binary dye mixture, and the slopes of the fitted lines were used to determine the effective diffusion coefficient D_p (m^2/s) and D_f (m^2/s).

Modeling of kinetic and isotherm data

The experimental kinetic data were fitted to the pseudo-first-order and pseudo-second-order kinetic models (Eqs. (9) and (10), respectively) (Brahmi et al. 2024).

$$q_t = q_e \times \left[1 - \exp\left(-k_1 t\right)\right], \tag{9}$$

$$q_t = q_e - \frac{q_e}{k_2 q_e t + 1}, \tag{10}$$

where k_1 (min^{-1}) denotes the pseudo-first-order rate constant and k_2 (g/(mg × min)) denotes the pseudo-second-order rate constant.

Three adsorption isotherm models, Langmuir, Freundlich, and Redlich–Peterson, were used to interpret the equilibrium data (Eqs. (11), (12), and (13), respectively) (Brahmi et al. 2024).

$$q_e = \frac{q_{\max} K_L C_e}{K_L C_e + 1}, \tag{11}$$

$$q_e = K_F C_e^{\frac{1}{n}}, \tag{12}$$

$$q_e = \frac{K_R C_e}{a_R C_c^{\beta} + 1}, \tag{13}$$

where $q_{\max}$ (mg/g) denotes the Langmuir monolayer adsorption capacity, K_L (L/mg) denotes the Langmuir adsorption constant, and K_F($mg^{1-\frac{1}{n}} \times L^{\frac{1}{n}}$/g) and $\frac{1}{n}$ denote the Freundlich constants and the partitioning coefficient, respectively, related to surface heterogeneity; K_R (L/g), a_R (L/mg), and β denote the Redlich–Peterson isotherm constants.

Furthermore, the validity of the data fitting to the isotherm models was evaluated using the root mean square error (RMSEC).

$$\text{RMSEC} = \sqrt{\frac{\sum_{i=1}^{n}\left(q_i^{\exp} - q_i^{\text{pred}}\right)^2}{N}}, \tag{14}$$

where $q_i^{\exp}$ and q_i^{pred} denote the obtained and predicted values of the adsorption amounts, respectively, and N represents the number of experiments. A lower RMSEC value indicates a good prediction capability of the model.

Box–Behnken optimization of regeneration parameters

The regeneration experiments were conducted using acetic acid for the G-PEG/SDS (L) granules and MB dye. The regeneration parameters were optimized using the BBD design while minimizing granule mass loss during the regeneration. Three independent variables were investigated: the acetic acid concentration (0.2–1 mol/L) (x_1), temperature (294–338 K) (x_2), and contact time (30–180 min) (x_3). The regeneration efficiency was calculated as weight-% of desorbed dye. The mass loss (as weight-%) was calculated after drying the regenerated granules overnight at 313 K.

Results and discussion

Morphological, microstructure, and mechanical properties of G-PEG/SDS granules

The FTIR spectra of HAP, MK-GP, and the granules prepared using PEG and SDS (solid or aqueous solution) are shown in Fig. 1. Each granule sample exhibits the characteristic absorption bands of both HAP (Meski et al. 2011; Ziani et al. 2014) and MK-GP (Luukkonen et al. 2019; Zenabou et al. 2019; Medri & Ruffini 2011). Furthermore, the peaks at 2841 and 1083 cm^{-1} (in the spectrum of G-PEG/SDS (S and L)) represent the symmetric stretching vibrations of the C–H bond and the stretching vibrations of the S = O bond of SDS (Zhang et al. 2023). This indicates that SDS was integrated into the granule structure and not removed during granule cleaning. The addition of SDS as a solid powder caused the stretching vibration of PO_4 tetrahedral units in HAP to shift from 1200 toward 1250 cm^{-1}, as observed in the spectra of G-PEG/SDS (S). Moreover, the XRF data show a slight decrease in the P content of the granule (Table S1, supporting information).

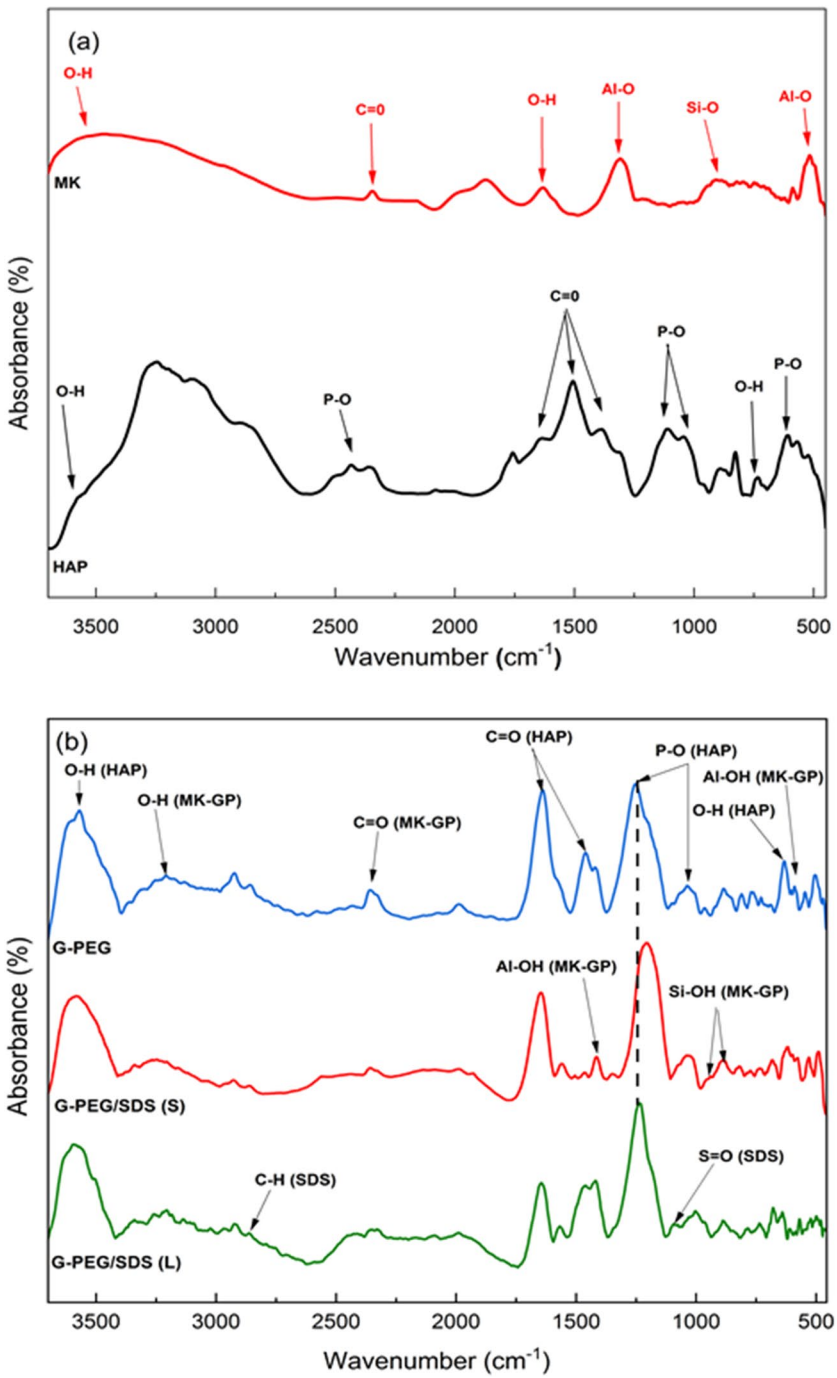

Fig. 1 FTIR spectra of **a** HAP and MK-GP powders and **b** G-PEG, G-PEG/SDS (S), and G-PEG/SDS (L) granules

This may be due to the dissolution of SDS during granule preparation by the addition of deionized water as a granulation fluid, resulting in an interaction between PO_4 groups of HAP and SO_4 groups of SDS.

Understanding how the elaborated granules react to temperature changes is critical for ensuring reliability, performance, and safety in a wide range of industrial applications. Moreover, it allows consideration of the appropriate approach to regenerate these granules (i.e., physical, chemical, or a combination of the two). The TGA and differential scanning calorimetry (DSC) thermograms shown in Fig. 2a, b illustrate the thermal behavior of HAP and MK-GP powders and the different elaborated granules.

According to the figures, the DSC and TGA thermograms of HAP powder (Fig. 2a) show two weight losses (12 and 9 wt%), accompanied by endothermic peaks

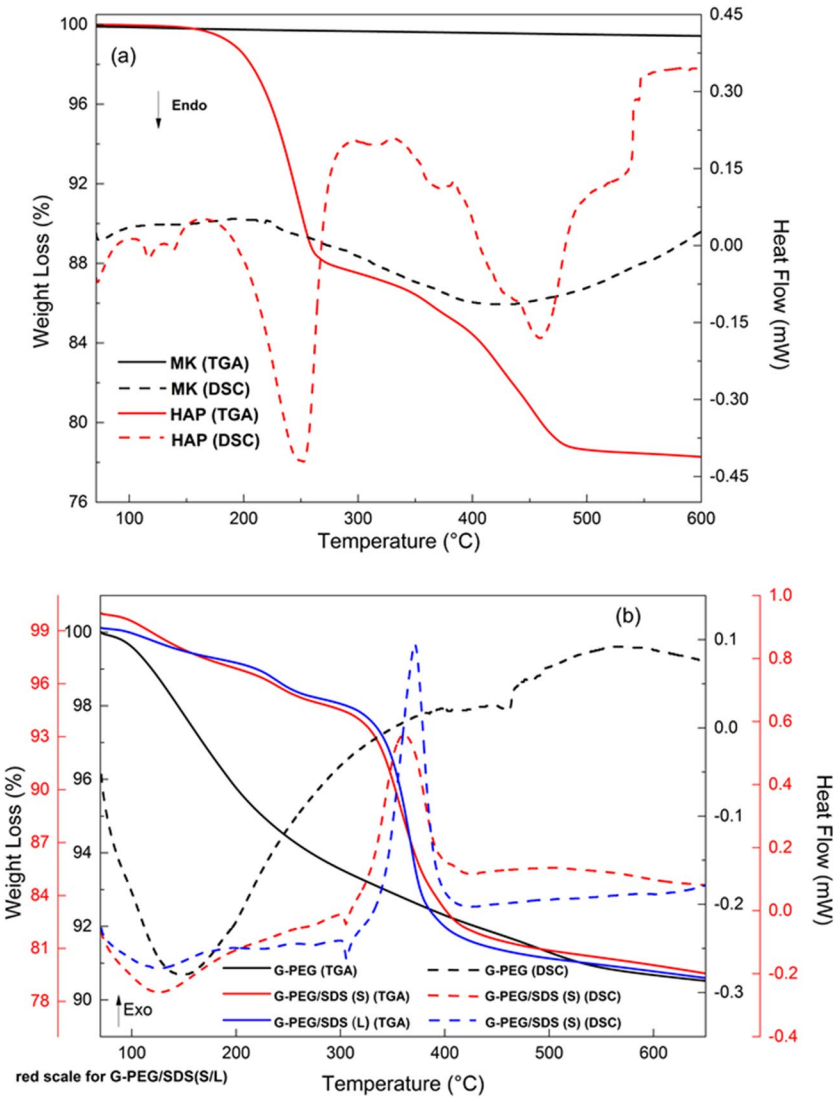

Fig. 2 TGA and DSC of **a** HAP and MK-GP powders and **b** G-PEG, G-PEG/SDS (S), and G-PEG/SDS (L) granules under nitrogen atmosphere

(at 250 °C and 470 °C). These weight losses are due to the evaporation of physisorbed and chemisorbed water molecules and the departure of synthesis residues. Above 480 °C, HAP generates a stable phase unlike MK, which records this stability throughout the range of heating temperature variation.

Moreover, as shown in Fig. 2b, the addition of SDS, either in liquid or solid form, to the G-PEG elaborated granules increases their decomposition by 8.79%. The increase in mass loss is mostly due to the disappearance of the long alkyl chain from SDS molecules (Lun et al. 2014). The presence of SDS reduces the surface tension of water, which can enhance its uniform dispersion into granules, thereby improving the process of removing PEG present in the granules and resulting in the elaboration of high-porosity granules.

The G-PEG/SDS (S/L) granules decompose in two steps: the first with 4 wt% in the 100–280 °C range, with an endothermic DSC signal at 120 °C, and the second with 14.5 wt%, with endothermic and exothermic DSC signals at 300 °C, 350 °C (the G-PEG/SDS (S)), and 370 °C (the G-PEG/SDS (L)). This is due to the loss of chemisorbed water molecules and the disappearance of the long alkyl chain from SDS molecules (Zhang et al. 2023). These findings suggest that chemical methods should be used to regenerate G-PEG/SDS (S/L) granules to prevent the breakdown of SDS.

The morphology of granules prepared using PEG and SDS (S or L) was assessed using SEM and optical microscopy. The results (Fig. 3) reveal highly porous granules with an asymmetric structure with a dense top layer and a porous sublayer with different pore sizes and forms.

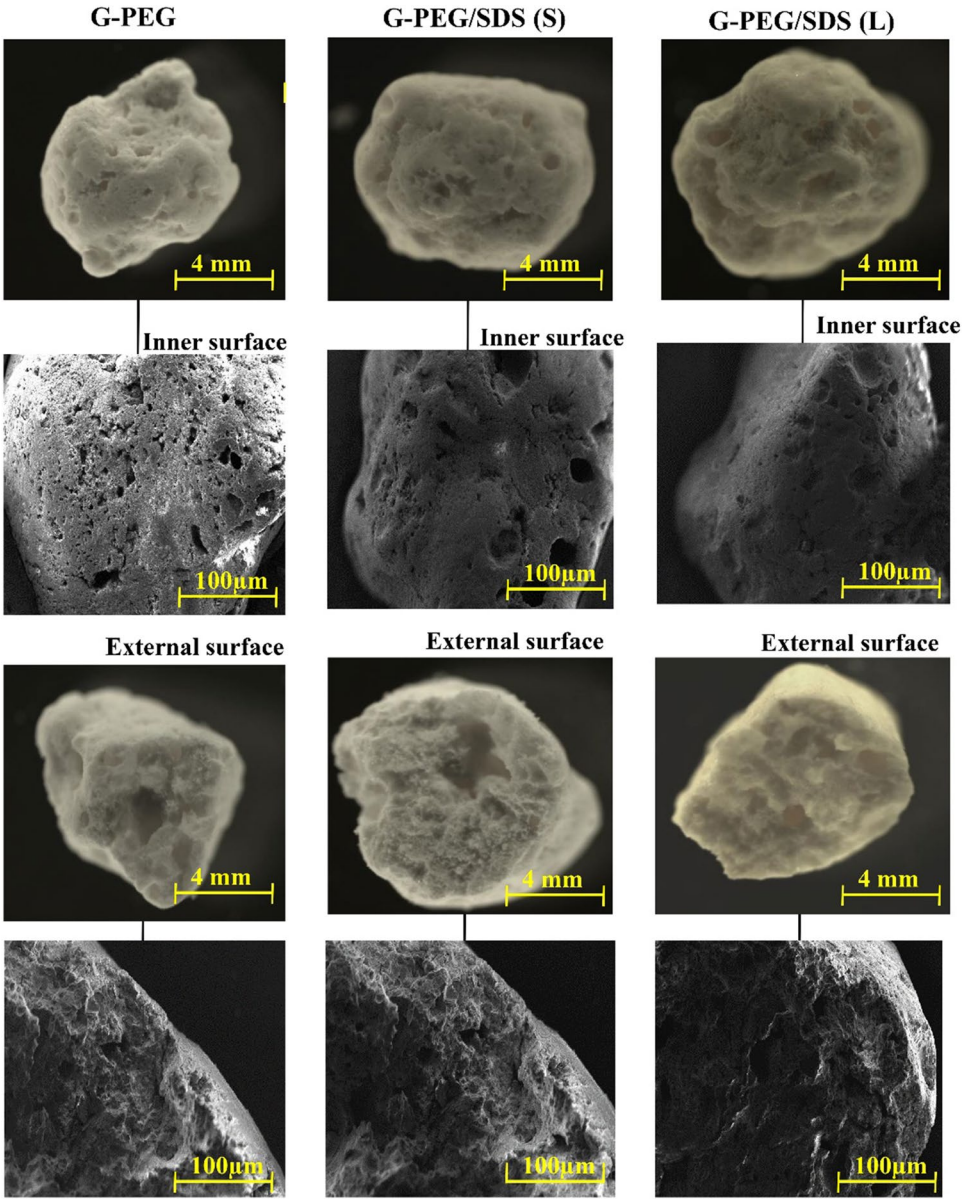

Fig. 3 SEM micrographs and optical microscope photographs of elaborated granules

The pore structure can be explained using the PEG removal process (described in the "Preparation of porous HAP-MK-PEG/SDS granules" section): at 358 K, PEG in the granules undergoes liquefaction, resulting in the formation of pores within the granules.

The N_2 adsorption/desorption isotherms and BJH pore size distribution for the HAP, MK, G-PEG, and G-PEG/SDS (S/L) granules are shown in Fig. S3 and Table 2, respectively.

The isotherms shown in Fig. S3 can be classified as type IV, indicating capillary condensation, and exhibit type H3 hysteresis, characteristic of mesoporous materials with irregular-shaped pores (Brahmi et al. 2024). This illustrates that the adsorption by the elaborated granules gradually increases from low pressures (approximately 0.01–0.45) and then sharply increases from 0.45 and above because of significant particle porosity. Comparing the volume adsorbed and the broadest desorption branch, the granules yield identical values and shapes.

However, the BJH pore size distribution (Fig. S3: inset) confirms that the mesopores (between 2 and 50 nm) dominate the pore structure of the granules (Brahmi et al. 2024).

Moreover, the granulation of the HAP and MK powders significantly affected their physical characteristics, altering particle arrangement, causing pore formation, influencing particle packing, and potentially creating a more complex

Table 2 Specific surface area, porosity, and mechanical parameters of HAP, MK, and the elaborated granules

Samples	G-PEG	G-PEG/SDS (S)	G-PEG/SDS (L)	HAP	MK
Average diameter d_0 (mm)	4.2 ± 0.1	4.1 ± 0.1	4.2 ± 0.1	–	–
Specific surface area (m^2/g)	73.08	85.25	97.89	31.20	10.74
Total pore volume (cm^3/g)	0.30	0.33	0.32	0.065	0.05
Mean pore diameter (nm)	16.79	15.89	13.27	11.82	21.82
F_{max} (N)	46.83 ± 0.4	44.31 ± 0.3	42.03 ± 0.6	–	–
Compressive strength (σ) (MPa)	0.91 ± 0.2	0.85 ± 0.4	0.81 ± 0.1	–	–
Deformation at F_{max} (%)	3.08 ± 0.3	4.26 ± 0.3	4.62 ± 0.4	–	–
Young's modulus (MPa)	16.69 ± 0.3	15.23 ± 0.2	15.08 ± 0.4	–	–

structure, which contributes to the observed increase in the specific surface area (Table 2 and Fig. S3).

Furthermore, the results reported in Table 2 indicate that the incorporation of SDS, either in liquid or solid form, into the G-PEG granules reduces the pore size and increases the surface area (an increase of 16% when solid SDS is used and 33% when dissolved SDS is used compared with granules without SDS). In general, a larger surface area implies improved adsorption properties.

The results of the mechanical compression test for the granules are displayed in Table 2. The G-PEG granules had the highest compressive strength and Young's modulus of 0.81 and 15.56 MPa, respectively. The higher mechanical strength is due to their lower porosity than that of the other granules (G-PES/SDS (S or L)).

Adsorption of MB and CV onto granules

The results of the comparative study between HAP, MK-GP, and the granules and the effect of SDS (S/L) on G-PEG granules are presented in Fig. 4. The results reveal that HAP alone does not adsorb either MB or CV dye. Conversely, MK-GP has an affinity to remove both dyes because of its negative surface charge. The granulation process of HAP and MK without SDS decreased the absorbed amount of MB and CV dyes compared with MK-GP. This can be explained by the decreased amount of MK-GP in the granules compared with that of MK-GP, which decreased the number of responsible active sites for MB and CV absorption.

However, the incorporation of SDS by dissolving it to a granulation fluid (i.e., G-PEG/SDS (L) granules) resulted in a synergistic increase in the adsorption of both MB and CV dyes compared with using HAP or MK-GP alone. Using the SDS solution as a granulation fluid reduces the

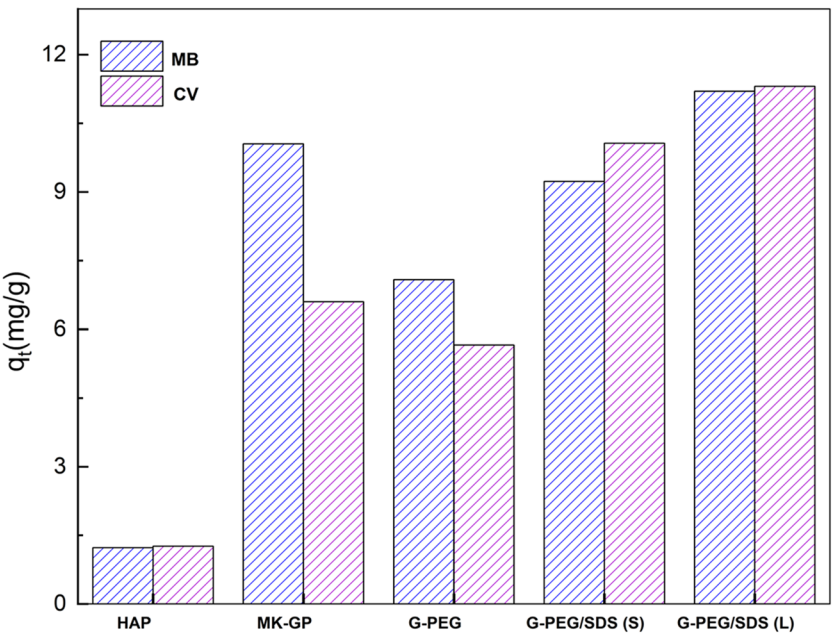

Fig. 4 Adsorption capacity of HAP, MK-GP, and elaborated granules for MB and CV dyes alone in aqueous solution. Conditions: $[dye]_0$ = 25 mg/L, granules mass = 2 g/L, pH of dye, $d_{granules}$ = 4 mm, agitation speed = 250 rpm, time = 90 min, and T = 298 K

surface tension of water, which can enhance its uniform dispersion into the forming granules, thereby leading to more efficient dissolution of sodium metasilicate and GP binder formation (Ramimoghadam et al. 2012). Moreover, this enhanced the porosity and surface area of the granules (Table 2) and improved the adsorption performance.

MB and CV dyes are weak bases with pK_a values of 2.6 and 9.4, respectively (i.e., they exist in the mono protonated (BH^+) and di-protonated (BH^{2+}) forms) (Lun et al. 2014; Li et al.2022). As pH increased, MB and CV uptake increased, reaching its maximum at pH = 8(Fig. 5a). This is due to the increased electrostatic attraction between the negatively charged granule surface (pH_{pzc} = 7.23 (Fig. 5b), i.e., the granules have a negative surface charge at pH higher than pH_{pzc}) and cationic MB and CV molecules.

Adsorption capacity and removal efficiency are influenced by the adsorbent dosage. Figure 5c shows that as the dosage increases from 1 to 3 g/L, the adsorption capacity increases to 18.6 and 23.3 mg/g for MB and CV, respectively.

Effect of dye concentration on adsorption

As shown in Fig. 6a, the adsorption of MB and CV dyes was faster during the first 5 min, and equilibrium was reached after 30 min. The quick equilibration time can be explained by the high porosity and specific surface area of the G-PEG/SDS (L) granules (as demonstrated by the SEM and BET/BJH results). Moreover, the adsorption amount of dyes significantly increased (from 7.3 to 34.8 mg/g for MB and from 7.4 to 45.2 mg/g for CV) as the initial dye concentration was increased. This can be ascribed to an increase in the driving power required to transport dye molecules from the solution to the solid surface (Bensedira et al. 2022).

Selectivity of G-PEG/SDS (L) granules toward dyes

The binary solutions of MB and CV dyes at different concentrations (15–100 mg/L, the original concentration ratio of each mixed dye in the solution was set to be 1:1) were used to evaluate the selectivity of G-PEG/SDS (L) granules for cationic dye adsorption under the aforementioned optimal conditions. The adsorption efficiency in the dye mixture solutions decreased compared with that in the individual solutions of each dye. This observed deviation is explained by the fact that both MB and CV dyes compete to occupy the available adsorption sites on the material surface. Moreover, the results indicate that, especially at concentrations higher than 50 mg/L, the granules had a stronger affinity for adsorbing CV than MB (Fig. 6b). This behavior can be attributed to the lower diffusion coefficient of CV than MB, as indicated in Table S2. When the dye concentrations are lower than 50 mg/L, both MB and CV have the same diffusion coefficients, because of less steric hindrance and a large concentration gradient; both MB and CV molecules are expected to move more swiftly within the

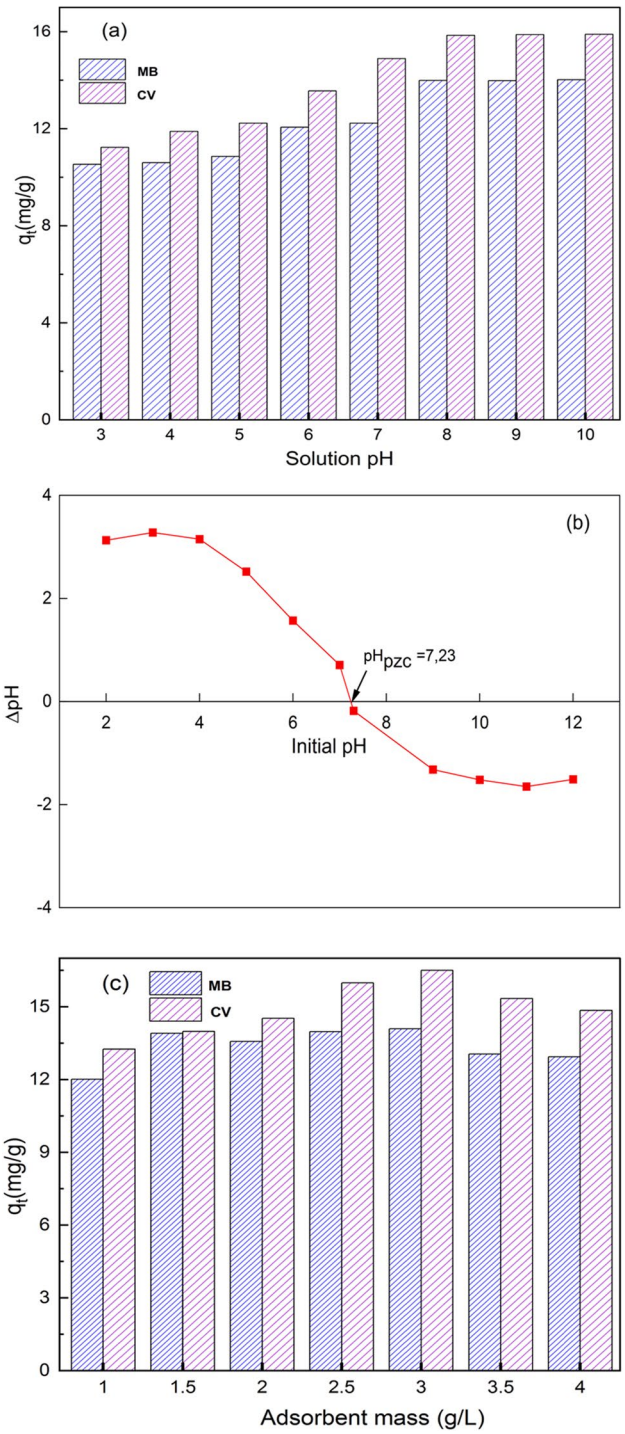

Fig. 5 **a** Effect of pH of solution on adsorption, **b** pH_{pzc} of granules, and **c** effect of granule mass per water volume on adsorption of MB and CV dyes alone in aqueous solution onto G-PEG/SDS (L). Conditions: $[dye]_0$ = 50 mg/L, $d_{granules}$ = 4 mm, agitation speed = 250 rpm, time = 90 min, and T = 298 K

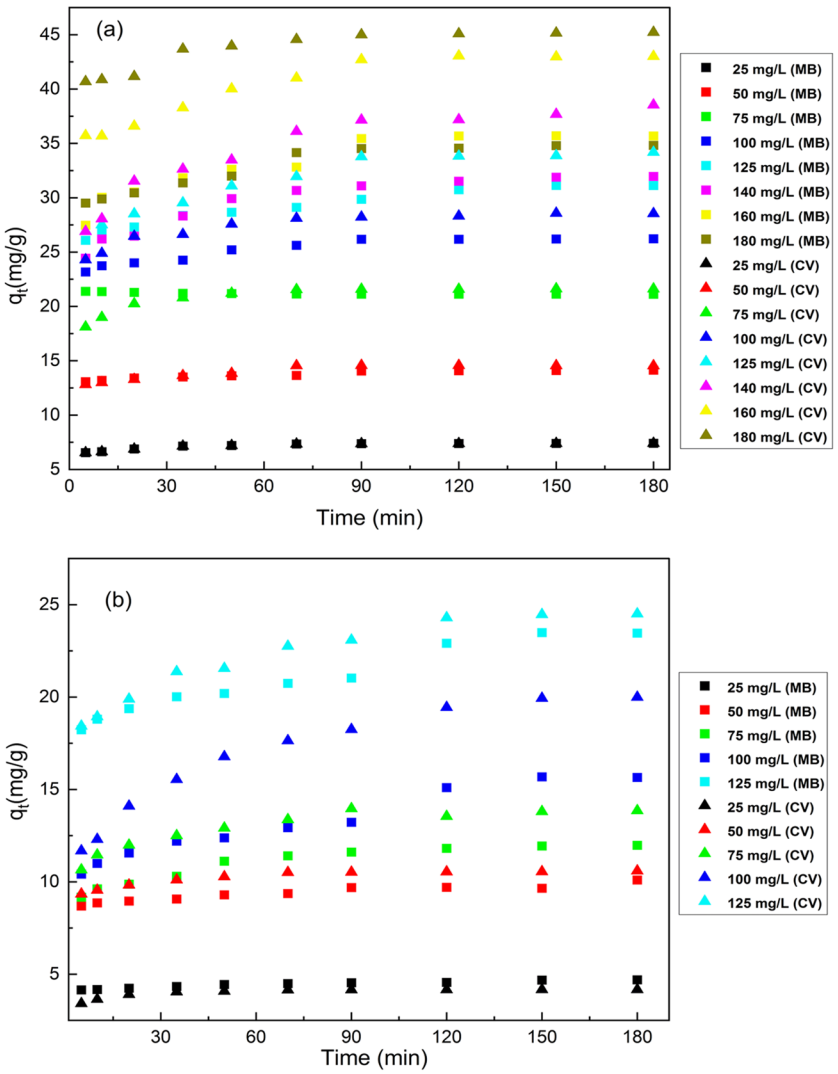

Fig. 6 Effect of initial concentration of MB and CV dyes on the adsorption amount onto G-PEG/SDS (L) granules. **a** Each dye alone in aqueous solution and **b** in binary dye mixtures. Conditions: pH = 8, adsorbent mass = 3 g/L, $d_{granules}$ = 4 mm, agitation speed = 250 rpm, time = 180 min, and T = 298 K

solution, leading to similar adsorption behaviors. However, as the concentration increases beyond 50 mg/L, the diffusion coefficient of CV dye becomes lower than that of MB dye, making it more difficult for MB molecules to diffuse through the solution and reach the granule surface. This can be attributed to the fact that the positively charged sites of CV molecules may interact more easily with the negatively charged surfaces of the granules compared with MB groups, facilitating CV diffusion.

Moreover, the separation factor values (Table 3) demonstrate that the granules have a stronger affinity for CV dye from a binary mixture than for MB dye.

Fitting of kinetic and adsorption isotherm models to data

Figure 7 and Table 4 illustrate the fitting of kinetic and isotherm models to the adsorption data on G-PEG/SDS (L) granules. The results indicate that the adsorption of MB and CV dyes, individually or in a binary mixture, onto the G-PEG/SDS (L) granules follows the pseudo-second-order kinetic model and Langmuir or Redlich–Peterson isotherms.

Table 3 Separation factors (α) for CV and MB in binary dye solution at various dye concentrations. Conditions: pH = 8, granule mass = 3 g/L, $d_{granules}$ = 4 mm, agitation speed = 250 rpm, time = 180 min, and T = 298 K

The initial concentrations of MB and CV in binary dye mixtures (mg/L)	$\alpha_{MB/CV}$	$\alpha_{CV/MB}$
25	0.95	0.97
50	1.02	1.12
75	0.41	2.38
100	0.49	2.01
125	0.89	1.11

MB/CV MB in binary dye mixture, *CV/MB* CV in binary dye mixture

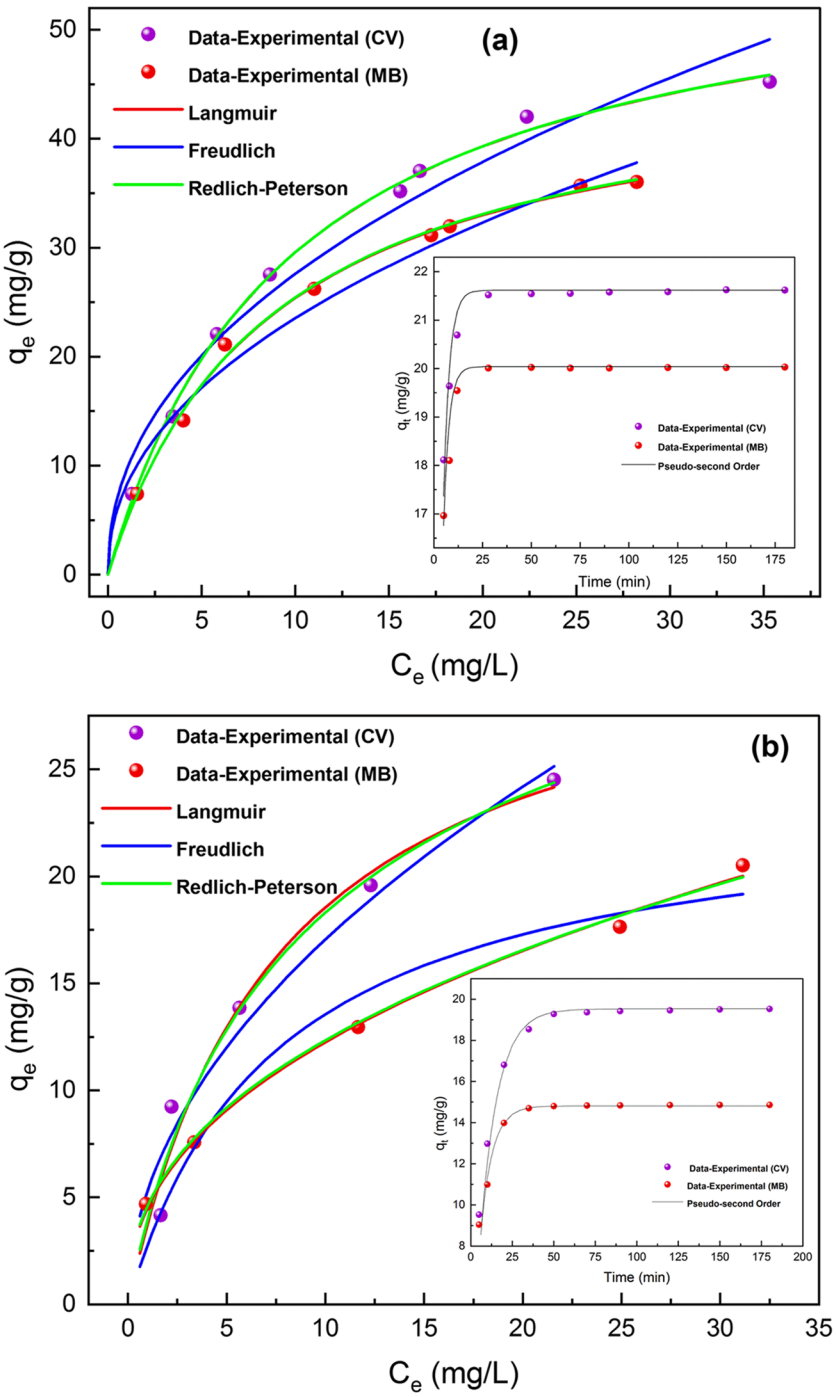

Fig. 7 Isotherm and kinetic models fitting to experimental data for MB and CV dyes **a** individually in aqueous solution and **b** in binary mixture. Conditions: pH = 8, adsorbent mass = 3 g/L, $d_{granules}$ = 4 mm, agitation speed = 250 rpm, time = 180 min, and T = 298 K

These findings suggest that the surface of the G-PEG/SDS (L) granules is homogeneous. All sites are equivalent, and each site can hold at most one cationic dye molecule (monolayer coverage only). There are no interactions between sorbate molecules on adjacent sites (Brahmi et al. 2024).

Experimental design and statistical analysis

Modeling of G-PEG/SDS (L) granule regeneration efficiency response

Statistical modeling was performed to investigate the effects of independent variables (i.e., acetic acid concentration, time, and temperature) and their mutual

Table 4 Kinetic and isotherm parameters for MB and CV dyes individually and in binary mixtures. Conditions: pH = 8, adsorbent dose = 3 g/L, $d_{granules}$ = 4 mm, agitation speed = 250 rpm, time = 180 min, and T = 298 K

		MB	MB/CV	CV	CV/MB
Kinetic model	Kinetic parameters				
Pseudo-first-order	q_{exp}(mg/g)	20.083	14.879	21.612	20.596
	q_{cal}(mg/g)	19.683	14.135	21.160	28.669
	k_1(min^{-1})	0.373	0.162	0.350	0.116
	R^2	0.973	0.943	0.956	0.963
Pseudo-second-order	q_{exp}(mg/g)	20.083	14.879	21.612	20.596
	q_{cal}(mg/g)	20.123	14.799	21.792	20.510
	k_2(mg/(g×L))	0.053	0.017	0.039	0.081
	R^2	0.992	0.995	0.990	0.994
Isotherm model		Equilibrium parameters			
Freundlich	$K_F(mg^{1-\frac{1}{n}}.L^{\frac{1}{n}}/g)$	8.216	4.531	9.634	5.328
	n^{-1}	0.457	0.436	0.451	0.550
	R^2	0.913	0.861	0.893	0.903
	RMSEC	0.383	0.170	0.623	0.210
Langmuir	K_L(mg/g)	0.116	0.136	0.102	0.130
	q_{max}(mg/g)	47.130	28.826	58.068	32.712
	R^2	0.992	0.991	0.997	0.998
	RMSEC	0.094	0.105	0.032	0.071
Redlich–Peterson	K_R(L/g)	5.510	2.897	5.618	4.765
	a_R(L/mg)	0.220	0.193	0.078	0.10
	B	0.983	0.884	1.001	0.992
	R^2	0.991	0.993	0.991	0.992
	RMSEC	0.194	0.189	0.138	0.081

MB/CV MB in binary mixtures (MB/CV), *CV/MB* CV in binary mixtures (MB/CV).

interactions on the regeneration efficiency of G-PEG/SDS (L) granules. In this context, a mathematical second-order quadratic polynomial model based on the RSM–BBD modeling was established using the experimental results of Table 5.

According to the analysis of variance data (Table S3), the adequacy of the proposed model to describe G-PEG/SDS (L) regeneration efficiency was confirmed by a small p-value (<0.05). Thus, the regression polynomial model for G-PEG/SDS (L) regeneration efficiency can be expressed as follows (Eq. (15), see Table 5 for the explanation of x_1, x_2, and x_3):

$$\hat{y} = 91.97 + 2.70x_1 - 3.76x_2 + 3.36x_3 - 1.86x_1x_2 - 12.32x_1x_3 - 4.36x_1^2 - 3.06x_2^2 - 4.37x_3^2. \quad (15)$$

Fig. S4 (a) illustrates the relationship between the measured and predicted G-PEG/SDS (L) regeneration efficiency. The data were distributed around a straight line ($R^2 = 0.99$), which unambiguously demonstrates the adequate correlation between the experimental and statistically predicted responses (AitAli et al. 2023). Furthermore, residual analysis, as shown in Fig. S4 (b), indicates that the predicted values and the residues have no relationship. Thus, the prediction model (Eq. (15)) can be used to explain the statistical results and predict the optimum conditions using RSM.

Study of model

The model discovered that all variables have an effect on granule regeneration ($p < 0.05$). The acetic acid concentration (x_1) and contact time (x_3) have a positive influence on desorption efficiency with coefficients $b_1 = 2.70$ and $b_3 = 3.36$, respectively, whereas the temperature has a negative influence ($b_2 = -3.76$). High temperatures accelerate the degradation of the granules, decreasing their structural integrity and performance.

Moreover, the regression model revealed the existence of slightly negative interactions between acetic acid concentration and temperature (x_{12}) and contact time (x_{13}).

To improve comprehension of the results, the predicted model (Eq. (15)) derived from BBD is illustrated in Fig. 8 as three-dimensional response surface plots. These plots, generated using MATLAB, serve to identify the optimal values of the operating parameters that yield the highest G-PEG/SDS (L) regeneration efficiency.

Figure 8a shows that an increase in acetic acid concentration (x_1) and contact time (x_3) positively influences the response, leading to an increase in G-PEG/SDS (L) regeneration efficiency. Extended contact times and elevated concentrations of acetic acid increased the diffusion of acetic acid within the granules, enhancing regeneration processes.

Furthermore, according to the curves shown in Fig. 8b, c, at high temperatures ($x_2 > 313$ K), it is recommended to minimize the contact time ($x_3 < 180$ min) and work with

Table 5 Experimental design matrix developed using RSM-based BBD model: variables, levels, and response

Values of parameters (coded experiment matrix)			Measured response	Predicted response	Residue
x_1, acetic acid concentration (mol/L)	x_2, temperature (K)	x_3, time (min)	y (%)	$\hat{y}$(%)	E
0.2 (−1)	298 (0)	180 (0)	90.36	89.86	0.5
0.2 (−1)	313 (0)	120 (−1)	64.25	64.83	−0.58
0.2 (−1)	313 (0)	240 (1)	95.86	96.21	−0.35
0.2 (−1)	328 (1)	180 (0)	86.53	86.07	0.46
0.6 (0)	298 (−1)	120 (−1)	90.56	90.46	0.1
0.6 (0)	298 (−1)	240 (1)	98.25	98.38	−0.13
0.6 (0)	313 (0)	180 (0)	92.69	91.97	0.72
0.6 (0)	313 (0)	180 (0)	91.25	91.97	−0.72
0.6 (0)	313 (0)	180 (0)	91.89	91.97	−0.08
0.6 (0)	313 (0)	180 (0)	92.05	91.97	0.08
0.6 (0)	328 (1)	120 (−1)	84.26	84.12	0.14
0.6 (0)	328 (1)	240 (1)	89.56	89.65	−0.09
1 (1)	298 (−1)	180 (0)	98.56	99.01	−0.45
1 (1)	313 (0)	120 (−1)	95.25	94.89	0.36
1 (1)	313 (0)	240 (1)	77.56	76.97	0.59
1 (1)	328 (1)	180 (0)	87.25	87.74	−0.49

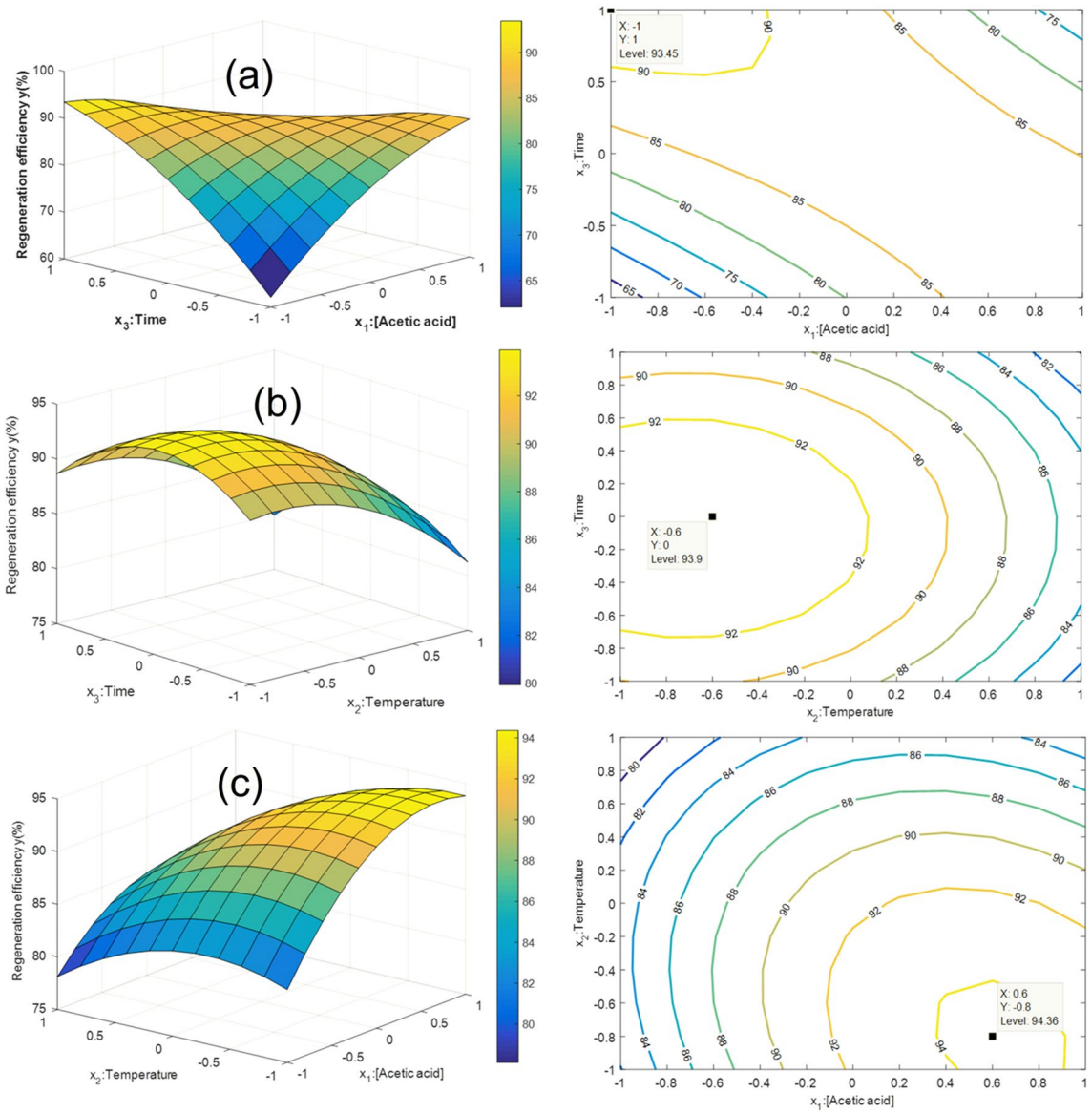

Fig. 8 Response surface and iso-response plots showing the effects of **a** acetic acid concentration and contact time, **b** temperature and contact time, and **c** acetic acid concentration and temperature on MB dye regeneration efficiency

a low acetic acid concentration ($x_1 < 0.6$ mol/L). As the temperature (x_2) and contact time (x_3) increase, the ratio of acetic acid inside the granules increases rapidly. This can cause a new reaction between the granule components (SDS, HAP, and MK-GP) and acetic acid, decreasing the number of active sites responsible for MB adsorption, thereby reducing regeneration efficiency. The optimal values were determined at an acetic acid concentration of 0.72 mol/L, a temperature of 323 K, and a contact time of 173.22 min. Duplicate confirmatory experiments were conducted using the optimized parameters. These parameters resulted in a measured regeneration rate of approximately 93.86% compared with the predicted granule regeneration rate of 90.89%.

G-PEG/SDS (L) granules were regenerated up to eight times without significant degradation (Fig. 9). However, after the eighth cycle, the rate of degradation increased because of treatment conditions, probably causing HAP dissolution.

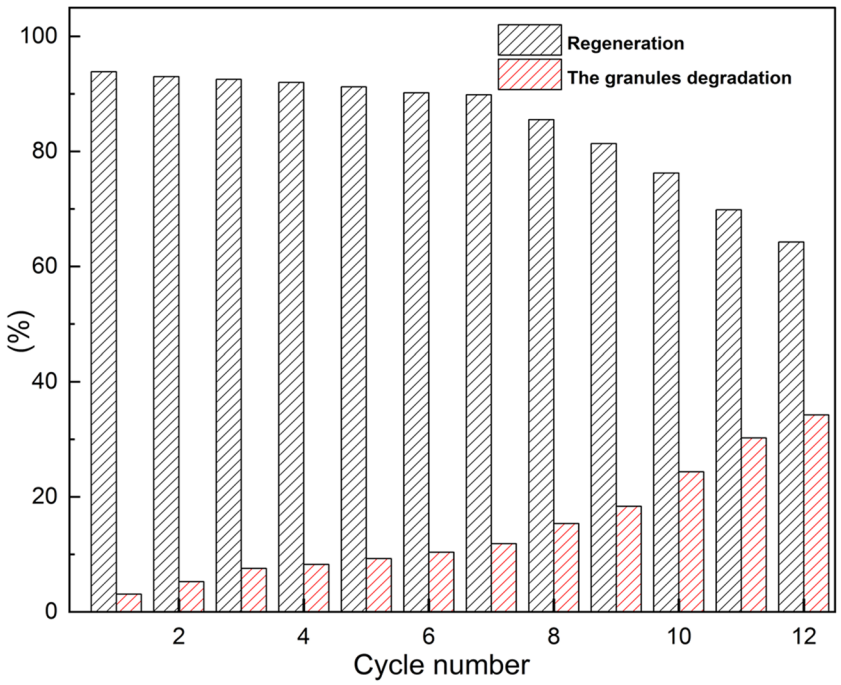

Fig. 9 Regeneration efficiency and granule degradation under optimal conditions: acetic acid concentration of 0.72 mol/L, temperature of 323 K, and contact time of 173.22 min

Comparison of the obtained granules with the previously developed adsorbents in the literature

This section compares the properties (i.e., surface area (SAA), adsorption capacity (q_{max}), and regeneration potential) of G-PEG/SDS (L) developed granules to traditional powdered adsorbents like MK-GP and HAP, as well as other relevant adsorbents in the literature. Table 6 summarizes the comparative analysis performed.

The results (Table 6) indicate that the G-PEG/SDS (L) developed granules have a high surface area and are cost-effective, making them a viable choice for industrial water treatment when compared to traditional powdered adsorbents, as well as

Table 6 Comparison of the properties of G-PEG/SDS (L) granules with the previously developed adsorbents in the literature

Adsorbent	Type	dyes	SAA (m^2/g)	q_{max}(mg/g)	Equilibrium time (min)	Regeneration	Ref
MK, HAP, PEG, SDS	Granules (4 mm)	MB	50–98	35	30 (298 K)	MB (8 cycle) CV (N/A)	This study
		CV		45			
MK, potassium-disilicate activating solution	Granules (2 mm)	MB	16	3–5	N/A	N/A	Medri et al. (2020)
Metakaolin and slag	Powder	MB	45	5	120 (298 K)	N/A	Feng et al. (2021)
MK-GP	Solid monolith	CV	27–62	27	120 (328 K)	N/A	Barbosa et al. (2018)
HAP	Powder	MB	N/A	26–38	20 (298 K)	N/A	Aaddouz et al. (2023)
Biochar-supported HAP	Powder	MB	26–127	21	800 (298 K)	4 cycles	Li et al. (2018)
Bio-HAP/MgO	Powder	CV	154	43	40 (298 K)	5 cycles	Foroutan et al. (2020)
Unmodifed HAp	Powder	CV	N/A	1	90 (298 K)	N/A	Amer Ali et al. (2023)
Other adsorbents							
Palm kernel fiber	Powder	CV	N/A	80	60 (298 K)	N/A	El-Sayed (2011)
		MB		95			
Zirconium silicate, SDS	Powder	CV	4–6	39	30 (298 K)	N/A	Mahmoud et al. (2019)
		MB		38			
Montmorillonite/magnetic Ni-Fe_2O_4-amine-functionalized chitosan	Powder	CV	N/A	118	30 (298 K)	10 cycles	Gomaa et al. (2022)
		MB		137			
CaO/g-C_3N_4-based nanocomposite	Powder	CV	N/A	458	240 (298 K)	N/A	Younis et al. (2016)
		MB		612			

other adsorbents. While some of these alternatives demonstrate superior adsorption capacity for removing MB and CV dyes, they face limitations in industrial applications primarily due to the challenges associated with handling powders. In addition, unlike G-PEG/SDS (L) granules, these alternative adsorbents can only be regenerated five times maximum.

MK metakaolin, *HAP* hydroxyapatite, *SDS* sodium dodecyl sulfate, *PEG* polyethylene glycol, *MB* methylene blue, *CV* crystal violet, *N/A* not variable

Conclusions

In this study, a novel granulation procedure was developed to obtain granules suitable for an adsorption application. The granulation method utilizes metakaolin geopolymer as a reactive binder for hydroxyapatite powder. The novel aspects are the use of PEG as a porogen agent and SDS dissolved in the granulation fluid (i.e., deionized water) which enhanced the granulation by reducing water surface tension. It should be noted that the proposed preparation method is versatile and can be applied to various geopolymers and alkali-activated materials, including lightweight artificial sound-absorbing acoustic panels, filtration materials, biofilm carrier materials, and catalyst support materials. It is expected to be simpler to scale and implement compared to previous methods (Valentina et al. 2020; Brahmi et al. 2024), and granule properties can be easily adjusted.

The adsorption selectivity study revealed that the G-PRG-SDS (L) granules exhibited higher adsorption toward CV than for MB. The maximum adsorption capacities (q_{max}) were 34.8 mg/g for MB and 45.2 mg/g for CV when the dyes were in present alone in an aqueous solution. In contrast, the maximum adsorption capacities were 23.5 mg/g for MB and 25.5 mg/g for CV when they were present together in a binary dye solution. Moreover, their adsorption either individually or in binary dye solutions followed the Langmuir isotherm model. The adsorption kinetic data indicated that the adsorption followed the pseudo-second-order kinetic model and was governed by film diffusion ($D_f = 1.37 \times 10^{-10}$ and 2.34×10^{-11} m^2/s for CV and MB dyes, respectively).

The optimization of the regeneration process of granules with acetic acid revealed that increasing the acid concentration and contact time improved the regeneration efficiency. The optimal values were 0.72 mol/L acetic acid concentration, 323 K, and 173 min contact time. Duplicate confirmatory experiments showed a regeneration rate of 94%, compared to the predicted rate of 91%. The granules could be regenerated for up to eight times without significant degradation. These results suggest that the porous granules prepared in this study have potential to be used in industrial wastewater treatment.

Recommendations for future work

The future research on the developed adsorbent granules should consider the following aspects:

- The granulation method could be still further developed by combining both PEG and SDS in the granulation fluid.
- The regeneration process by combining a chemical and thermal approach could be explored.
- The adsorption capacity of the granules may be too low if treating wastewater containing a high load of dyes. Thus, adsorption alone may not be sufficient as a treatment process. Therefore, combining adsorption with other methods such as electrocoagulation (Al-Qodah et al. 2024), biological treatment and others should be considered for future studies to enhance the treatment efficiency.

Supplementary Information The online version contains supplementary material available at https://doi.org/10.1007/s11356-024-34001-6.

Author contributions Aghilas Brahmi: conceptualization, formal analysis, investigation, methodology, validation, visualization, and writing—original draft. Salima Ziani: methodology, supervision, writing—review and editing, and conceptualization. Salima AitAli: conceptualization, methodology, supervision, and writing—review and editing. Hafit Khireddine: review and editing. Tero Luukkonen: conceptualization, funding acquisition, methodology, resources, supervision, and writing—review and editing.

Data availability Not applicable.

Declarations

Ethics approval Not applicable.

Consent to participate Not applicable.

Consent for publication Not applicable.

Conflict of interest The authors declare no competing interests.

References

Aaddouz M, Azzaoui K, Akartasse N, Mejdoubi E, Hammouti B, Taleb M, Sabbahi R, Alshahateet SF (2023) Removal of methylene blue from aqueous solution by adsorption onto hydroxyapatite nanoparticles. J Mol Struct 1288:135807. https://doi.org/10.1016/j.molstruc.2023.135807

AitAli S, Ziani S, Yahiaoui I, Brahmi A, Boudrahem F, Aissani-Benissad F (2023) Application of central composite design and response surface methodology for the study of extraction of gentian violet dye in aqueous solution by polystyrene membrane modified with oleic acid. Environ Prog Sustain Doi. https://doi.org/10.1002/ep.14200

Al-Qodah Z, Al-Zghoul TM, Jamrah A (2024) The performance of pharmaceutical wastewater treatment system of

electrocoagulation assisted adsorption using perforated electrodes to reduce passivation. Environ Sci Pollut Res 31:20434–20448. https://doi.org/10.1007/s11356-024-32458-z

Amer Ali D, Saad FA, Elsawy H (2023) Kinetics and isotherm studies for adsorption of gentian violet dye from aqueous solutions using synthesized hydroxyapatite (T Liu, Ed.). J Environ Res Public Health 2023:1–15. https://doi.org/10.1155/2023/7418770

Barbosa TR, Foletto EL, Dotto GL, Jahn SL (2018) Preparation of mesoporous geopolymer using metakaolin and rice husk ash as synthesis precursors and its use as potential adsorbent to remove organic dye from aqueous solutions. Ceram Int 44:416–423. https://doi.org/10.1016/j.ceramint.2017.09.193

Benamor M, Bouariche Z, Belaid T, Draa MT (2008) Kinetic studies on cadmium ions by Amberlite XAD7 impregnated resins containing di(2-ethylhexyl) phosphoric acid as extractant. Separation Purification Technol 59:74–84. https://doi.org/10.1016/j.seppur.2007.05.031

Boyd GE, Adamson AW, Myers LS (1947) The exchange adsorption of ions from aqueous solution by organic zeolites. II Kinetics. J Am Chem Soc 69:2836–2848. https://doi.org/10.1021/ja01203a066

Chen Y (2023) Key factors improving the stability and the loading capacity of nitrogen removal in a hydroxyapatite (HAP)-enhanced one-stage partial nitritation anammox process. Chem Eng J 452:139589. https://doi.org/10.1016/j.cej.2022.139589

El-Sayed GO (2011) Removal of methylene blue and crystal violet from aqueous solutions by palm kernel fiber. Desalination 272:225–232. https://doi.org/10.1016/j.desal.2011.01.025

Feng X, Yan S, Jiang S, Huang K, Ren X, Du X, Xing P (2021) Green synthesis of the metakaolin/slag based geopolymer for the effective removal of methylene blue and Pb (II). SILICON 14:6965–6979. https://doi.org/10.1007/s12633-021-01439-z

Foroutan R, Peighambardoust SJ, Aghdasinia H, Mohammadi R, Ramavandi B (2020) Modification of bio-hydroxyapatite generated from waste poultry bone with MgO for purifying methyl violet-laden liquids. Environ Sci Pollut Res 27:44218–44229. https://doi.org/10.1007/s11356-020-10330-0

Huang B, Xiong D, Zhao T, He H, Pan X (2016) Adsorptive removal of PPCPs by biomorphic HAP templated from cotton. Water Sci Technol 74:276–286. https://doi.org/10.2166/wst.2016.209

Li Y, Zhang Y, Zhang Y, Wang G, Li S, Han R, Wei W (2018) Reed biochar supported hydroxyapatite nanocomposite: characterization and reactivity for methylene blue removal from aqueous media. J Mol Liq 263:53–63. https://doi.org/10.1016/j.molliq.2018.04.132

Li Y, Otsubo M, Kuwano R (2022) Interpretation of static and dynamic Young's moduli and Poisson's ratio of granular assemblies under shearing. Computers and Geotechnics 142:104560. https://doi.org/10.1016/j.compgeo.2021.104560

Liu N, Wang H, Weng C, Hwan C (2008) Adsorption characteristics of Direct Red 23 azo dye onto powdered tourmaline. Sep Purif Technol 59:74–84. https://doi.org/10.1016/j.arabjc.2016.04.010

Lun H, Ouyang J, Yang H (2014) Enhancing dispersion of halloysite nanotubes via chemical modification. Phys Chem Minerals 41:281–288. https://doi.org/10.1007/s00269-013-0646-9

Luukkonen T, Heponiemi A, Runtti H, Pesonen J, Lassi U (2019) Application of alkali-activated materials for water and wastewater treatment: a review. Rev Environ Sci Biotechnol 18:271–297. https://doi.org/10.1007/s11157-019-09494-0

Mahmoud ME, Nabil GM, Khalifa MA, El-Mallah NM, Hassouba HM (2019) Effective removal of crystal violet and methylene blue dyes from water by surface functionalized zirconium silicate nanocomposite. J Environ Chem Eng 7:103009. https://doi.org/10.1016/j.jece.2019.103009

Manatunga DC, De Silva RM, De Silva KMN, De Silva N, Premalal EVA (2018) Metal and polymer-mediated synthesis of porous crystalline hydroxyapatite nanocomposites for environmental remediation. R Soc Open Sci 171557:1–15. https://doi.org/10.1098/rsos.171557

Medri V, Ruffini A (2011) The influence of process parameters on in situ inorganic foaming of alkali-bonded SiC based foams. Ceram Int 38:3351–9. https://doi.org/10.1016/j.ceramint.2011.12.045

Medri V, Papa E, Lizion J, Landi E (2020) Metakaolin-based geopolymer beads: production methods and characterization. J Clean Prod 244:118844. https://doi.org/10.1016/j.jclepro.2019.118844118844

Meski S, Ziani S, Khireddine H, Boudboub S, Zaidi S (2010) Factorial design analysis for sorption of zinc on hydroxyapatite. J Hazard Mater 186:1007–1017. https://doi.org/10.1016/j.jhazmat.2010.11.087

Meski S, Ziani S, Khireddine H, Yataghane F, Ferguene N (2011) Elaboration of the hydroxyapatite with different precursors and application for the retention of the lead. J Water Sci Technol 63:2087–2096. https://doi.org/10.2166/wst.2011.210

Panneerselvam K, Arul KT, Warrier AR (2019) Rapid adsorption of industrial pollutants using metal ion doped hydroxyapatite. AIP Conf Proc 2117:020004. https://doi.org/10.1063/1.5114584

Peng X, Chen W, He Z, Li D, Liu H, Jin H, Zhou G, Xu F (2019) Removal of Cu (II) from wastewater using doped HAP-coated-limestone. Journal of Molecular Liquids 293:111502. https://doi.org/10.1016/j.molliq.2019.111502

Ramimoghadam D, Mohd ZBH, Yun HTY (2012) The effect of sodium dodecyl sulfate (SDS) and cetyltrimethylammonium bromide (CTAB) on the properties of ZnO synthesized by hydrothermal method Int. J. Mol. Sci. 13:13275–13293. https://doi.org/10.3390/ijms131013275

Shen J, Wang X, Zhang L, Yang Z, Yang W, Tian Z, Chen J, Tao T (2018) Size-selective adsorption of methyl orange using a novel nano-composite by encapsulating HKUST-1 in hyper-crosslinked polystyrene networks. J Clean Prod 184:949–958. https://doi.org/10.1016/j.jclepro.2018.03.015

Teymouri A (2018) Hydroxyapatite and dittmarite precipitation from algae hydrolysate. Algal Research 29:202–211. https://doi.org/10.1016/j.algal.2017.11.030

Wang Y, Hu L, Zhang G, Yan T, Yan L, Wei Q, Du B (2017) Removal of Pb(II) and methylene blue from aqueous solution by magnetic hydroxyapatite-immobilized oxidized multi-walled carbon nanotubes. J Colloid Interface Sci 494:380–388. https://doi.org/10.1016/j.jcis.2017.01.105

Younis CA, Abd-Elaziz A, Hashem AI (2016) Utilization of a pyrrole derivative based antimicrobial functionality impregnated onto CaO/g-C3N4 for dyes adsorption. RSC Adv 6:89367–89379. https://doi.org/10.1039/C6RA10143G

Yu L, Luo YM (2014) The adsorption mechanism of anionic and cationic dyes by Jerusalem artichoke stalk-based mesoporous activated carbon. J Environ Chem Eng 2:220–229. https://doi.org/10.1016/j.jece.2013.12.016

Zhang X, Bai C, Qiao Y, Wang X, Jia D (2021) Porous geopolymer composites: a review. Composites Part A 150:106629. https://doi.org/10.1016/j.compositesa.2021.106629

Ziani S, Meski S, Khireddine H (2014) Characterization of magnesium-doped hydroxyapatite prepared by sol-gel process. Int J Appl Ceram 11:83–91

Al Natsheh A, Gray A, Luukkonen T (2022) Drivers and barriers for productization of alkali-activated materials in environmental technology, in: T. Luukkonen (Ed.), Alkali-Activated Materials in Environmental Technology Applications, Woodhead Publishing, Sawston, pp. 407–426, 10.1016/B978-0-323-88438–9.00008–9

Bensedira A, Haddaoui N, Doufnoune R, Meziane O, Labidi NS (2022) Study of methylene blue dye elimination from water using polyaniline (PANI) and PANI/SiO_2 composite. J Polym PolymCompos 30. https://doi.org/10.1177/09673911221141747

Brahmi A, Ziani S, AitAli S, Benkhaoula BN, Yu Y, Hania A, Khireddine H, Luukkonen T (2024) Porous metakaolin geopolymer as a reactive binder for hydroxyapatite adsorbent granules in dye removal. Hybrid Advances. https://doi.org/10.1016/j.hybadv.2023.100134

Gomaa H, Abd El-Monaem E M, Eltaweil A S, Omer AM (2022) Efficient removal of noxious methylene blue and crystal violet dyes at neutral conditions by reusable montmorillonite/NiFe2O4@amine-functionalized chitosan composite. Sci Rep 12. https://doi.org/10.1038/s41598-022-19570-1.

Luukkonen T, Yliniemi J, Sreenivasan H, Ohenoja K, Finnilä M, Franchin G, Colombo P (2020) Ag-or Cu-modified geopolymer filters for water treatment manufactured by 3D printing, direct foaming, or granulation. Sci Rep 101–14. https://doi.org/10.1038/s41598-020-64228-5

Zenabou NNM, Benoit-ali N, Zekeng S, Rossignol S, Melo UC, Tchamba AB (2019) Improving insulation in metakaolin based geopolymer: Effects of metabauxite and metatalc 23:403–15. https://doi.org/10.1016/j.jobe.2019.01.012.

Zhang J, Qi Y, lv T, Niu X, Tai B (2023) Effects of sodium dodecyl sulfate on nano carbon black-filled cement paste: performance and microstructure. J Mater Res Technol 24: 1706 e 1715. https://doi.org/10.1016/j.jmrt.2023.03.055

Authors and Affiliations

Aghilas Brahmi[1,2] · Salima Ziani[1,3] · Salima AitAli[1,3] · Hafit Khireddine[3] · Tero Luukkonen[2,4]

✉ Aghilas Brahmi
a.brahmi@univ-bouira.dz

[1] Laboratoire Des Matériaux Et Développement Durables (LMDD), Département de Génie Des Procédés, Faculté Des Sciences Et Des Sciences Appliquées, Université A.M.O, Bouira 10000, Algeria

[2] Fibre and Particle Engineering Research Unit, University of Oulu, P.O. Box 4300, Oulu 90014, FI, Finland

[3] Laboratoire de Génie de LEnvironnement (LGE), Faculté de Technologie, Université A. MIRA, Route de Targua Ouzemour, Bejaia 06000, Algeria

[4] Department of Chemical Engineering Technology, University of Johannesburg, P.O. Box 17011, Doornfontein 2088, South Africa